Supporting Information

Silica-based SERS Chip for Rapid and Ultrasensitive Detection of Fluoride Ion by Triggered Cyclic Boronate Ester Cleavage Reaction

Jian Zhang,*[,a] Lifang He,[a] Peirong Chen,[a] Chao Tian,[a] Jianping Wang,[b] Bianhua Liu,[b] Changlong Jiang,*[,b] and Zhongping Zhang[b.c]

[a] Department of Applied Chemistry, Anhui Agricultural of University, Hefei, Anhui 230036, China.

[b]CAS Center for Excellence in Nanoscience, Institute of Intelligent Machines, Chinese Academy of Sciences, Hefei, Anhui 230031, China

[c]School of Chemistry and Chemical Engineering, Anhui University, Hefei, Anhui 230601, China

*To whom correspondence should be addressed. E-mail: jianzhang@ahau.edu.cn; cljiang@iim.ac.cn. Fax: (+86) 551-65591156.

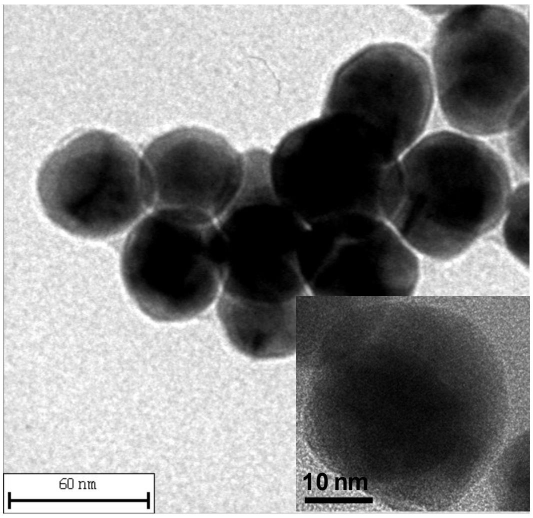

Fig. S1 TEM and HRTEM images of the prepared Au@Ag NPs.

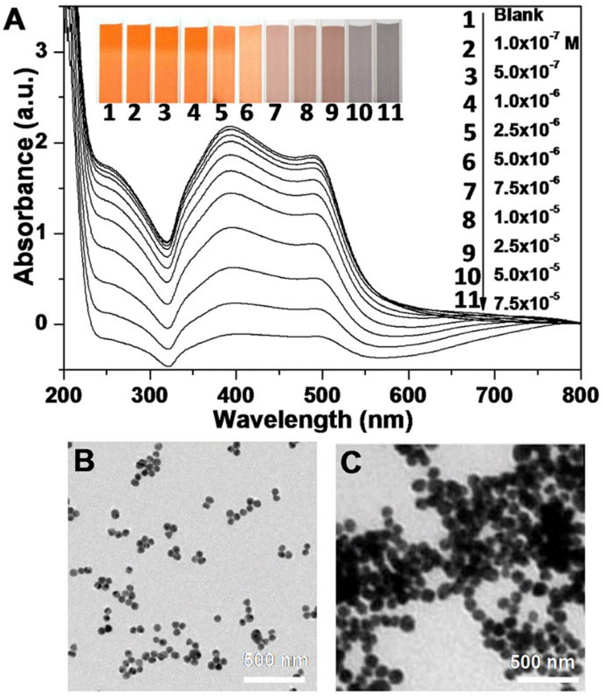

Fig. S2 (A) UV-vis absorption spectra of Au@Ag NPs colloid with the increase of Diol concentration from 1.0×10^{-7} to 7.5×10^{-5} M. The TEM images of Au@Ag NPs states (B) in the absence and (C) in the presence of 7.5×10^{-5} M Diol.

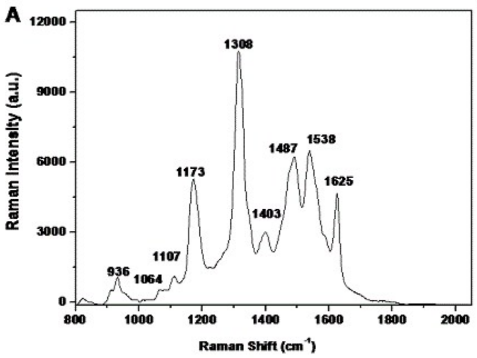

B

SERS bands	Vibrational modes
936	C-C in-plane bending
1064	C-C in-plane bending coupled with C-B
1107	C-H in-plane bending of xanthene ring
1173	C-H in-plane bending of xanthene ring
1308	C-H in-plane bending of xanthene ring
1403	xanthene ring stretching
1487	xanthene ring stretching
1538	nontotally symmtetric ring stretching
1625	totally symmtetric ring stretching

Fig. S3 (A) SERS spectra of the pure Flu-PBA (the strong Raman peaks at 936, 1064, 1107, 1173, 1308, 1403, 1487, 1538 and 1625cm^{-1} are the same as that of Flu-PBA-Diol-Au@Ag NPs). (B) The SERS bands of the Flu-PBA and their vibrational mode assignments SERS bands.

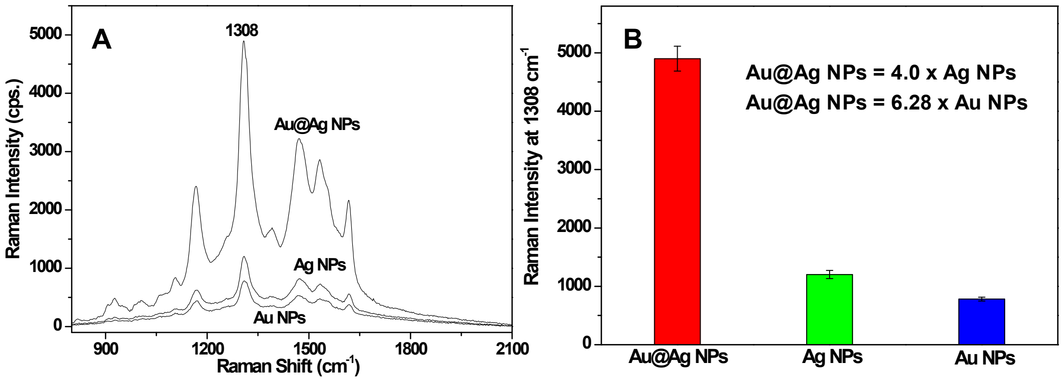

Fig. S4 (A) SERS spectra of Flu-PBA-Diol-Au@Ag, Flu-PBA-Diol-Ag and Flu-PBA-Diol-Au NPs colloids, and (B) the comparison of enhancement effects of the three metal particle colloids. It can be estimated that the enhancement effect of Au@Ag NPs is ~6.28- and 4.0-fold those of pure Au and Ag NPs.

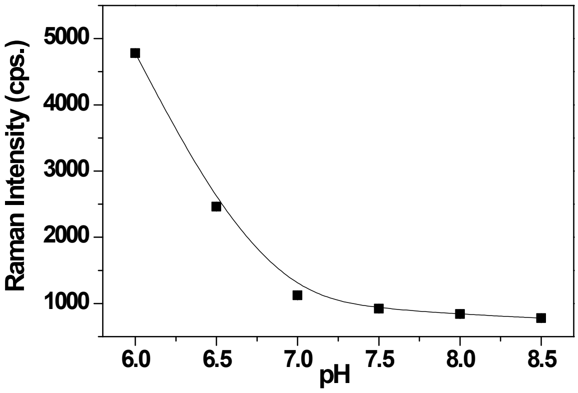

Fig. S5 The variation of Raman intensity of Flu-PBA-Diol-Au@Ag NPs at 1308 cm^{-1} with increasing pH values from 6.0 to 8.5. The conditions: 1.0 mL probe, 1.0 µM F^-.

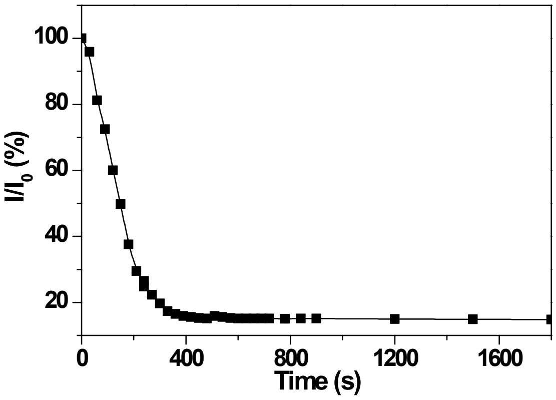

Fig. S6 The variation of Raman intensity of Flu-PBA-Diol-Au@Ag NPs at 1308 cm^{-1} with increasing incubation time after the addition of F^-. The conditions: 1.0 mL probe, 1.0 µM F^-, pH 7.4.

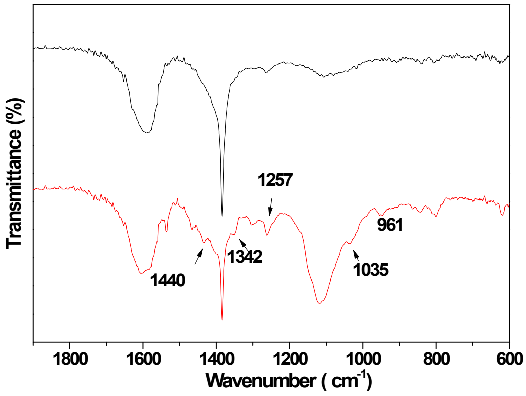

Fig. S7 FTIR spectra of Flu-PBA-Diol-Au@Ag NPs (a) and the resulted Diol-Au@Ag NPs after centrifugation in the presence of F^-(b).

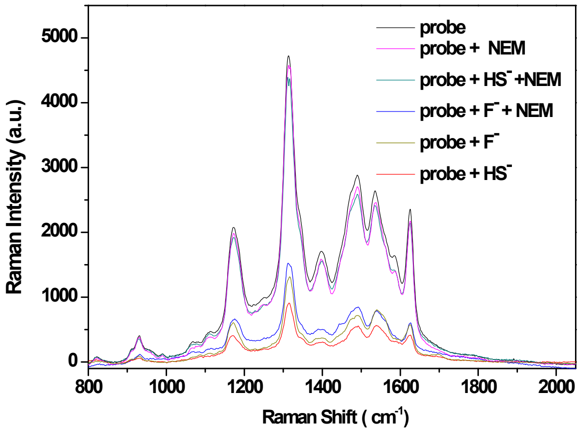

Fig. S8 SERS responses of Flu-PBA-Diol-Au@Ag NPs probe to F^-, HS^-, NEM, F^-+NEM, and HS^- +NEM (F^-: 1.00 μM; HS^-: 1.00 μM; NEM: 1.00 μM). The addition of NEM can effectively eliminate the interference of HS^-.

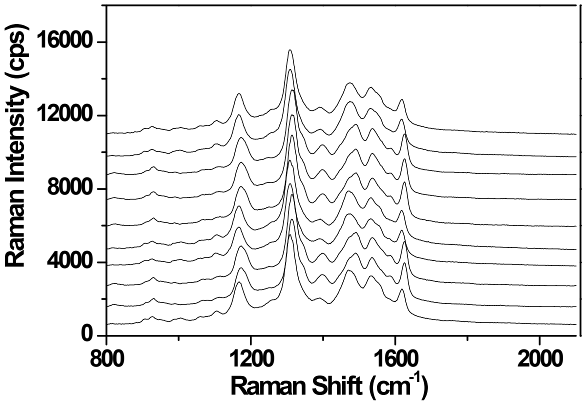

Fig. S9 A series of SERS spectra obtained from the randomly selected 10 sites of the assembled SERS chip.

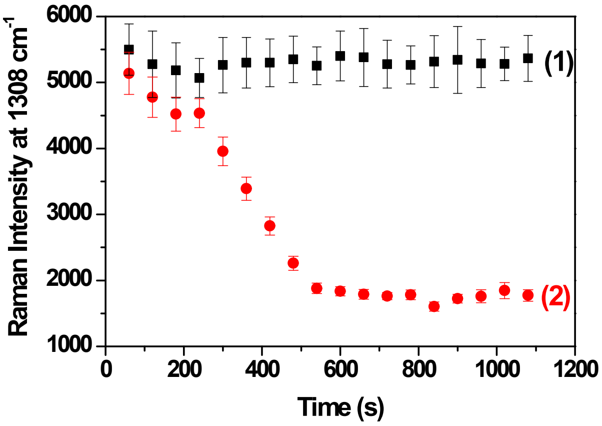

Fig. S10 The variation of Raman intensity at 1308 cm^{-1} (the data were collected at the interval of 60 s) by dropping 20 μL of (1) pure water and (2) 5.0×10^{-7} M F^- onto the assembled SERS chip.

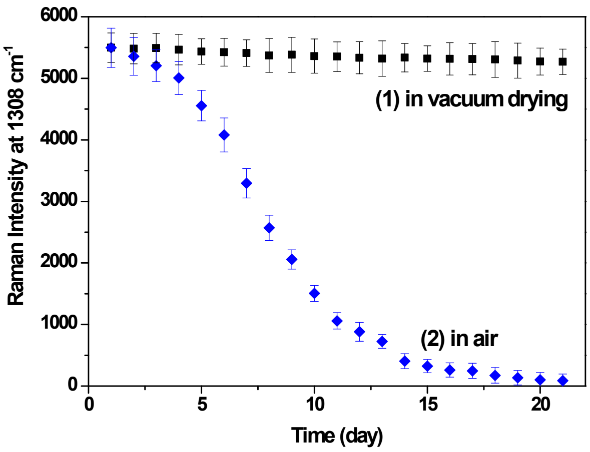

Fig. S11 The variation of Raman intensity of the assembled SERS chip at 1308 cm^{-1} (the data were collected at the interval of 1 day) in the different conditions: (1) in vacuun drying and (2) in air.

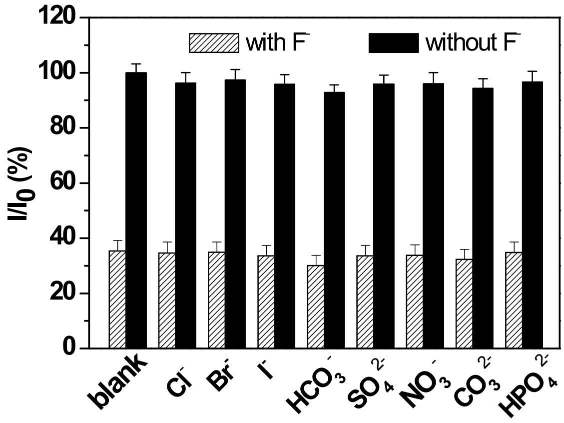

Fig. S12 The selectivity of the silica-based SERS chip in addition of the other anions (1.0×10^{-5} M) without and with the coexistence of F$^-$ (1.0×10^{-6} M). (I and I$_0$ represent the Raman intensity at 1308 cm^{-1} in the presence and absence of analytes, respectively).

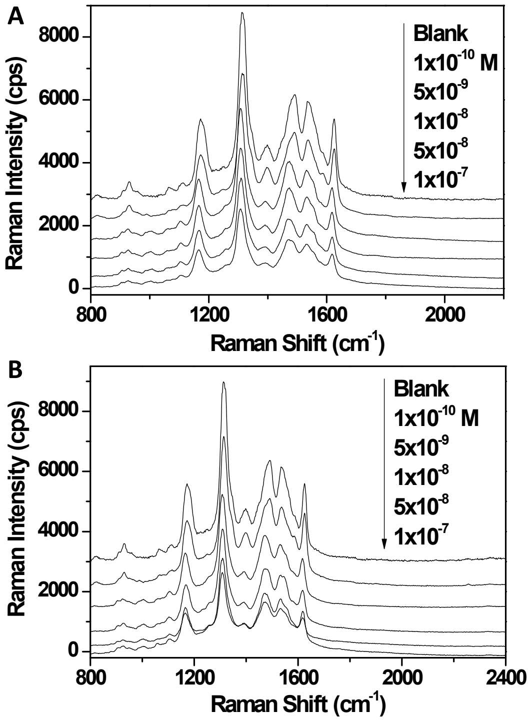

Fig. S13 SERS detections of F^- spiked with the different concentrations in (A) tap water, (B) lake water on the assembled SERS chip.